研究論文

Density Profile and Fluctuation Measurements Using Microwave Reflectometry

MASE Atsushi*, TOKUZAWA Tokihiko※, BRUSKIN Leonid G., KOGI Yuichiro, KUBOTA Shigeyuki, OYAMA Naoyuki, ONUMA Tsuyoshi, GOTO Naoki, ITAKURA Akiyosi, ICHIMURA Makoto, HOJO Hitoshi, TAMANO Teruo and YATSU Kiyoshi
Plasma Research Center, University of Tsukuba, Tsukuba 305-8577, Japan

(Received 8 June 1998/Accepted 21 July 1998)

Abstract

The microwave reflectometers on GAMMA 10 measure the density profile and fluctuations in the central-cell plasma. The density profile measurement using a broadband reflectometer is performed for various sweep times of the oscillator, 5 ms − 5 μs. The reliability of the measurements seems to be improved when the sweep time is faster than 50 − 100 μs. The resultant intermediate frequencies from a mixer output of the reflectometer are larger than 1 MHz. The several reconstruction algorithms are used to analyze the fast time-varying data, such as, the maximum-entropy method (MEM) and wavelet analysis as well as the standard zero-cross fringe counting method. The integrated value of many reconstructed density profiles agrees well with the profile obtained from a scanning interferometer. The proof-of-principle experiment of an ultrashort-pulse reflectometry is also performed.

The reflectometer is also applied to the measurement of density/magnetic fluctuations. The space- and time-resolving spectra of ICRF-driven waves as well as low-frequency waves are obtained. The density and magnetic-field fluctuation levels are evaluated from both the reflectometer and cross-polarization scattering (CPS) diagnostic method which is related to the mode-conversion effect consisting of a polarization difference of a scattered wave with regard to an incident wave by existence of magnetic fluctuations. It is observed that the Bragg resonance condition seems to be satisfied for the CPS similar to conventional Thomson scattering.

Keywords:

microwave diagnostics, reflectometry, density profile, density fluctuation, magnetic fluctuation

1. Introduction

Reflectometry has been expected to be one of the key diagnostics to measure density profiles and density/magnetic-field fluctuations in large fusion devices. It provides good spatial and temporal resolutions, while requiring a single viewing chord and minimal vacuum access in contrast to interferometry and Thomson scattering. One of the most serious problems in density profile measurement using conventional frequency-modulation (FM) reflectometer is caused by the existence of density fluctuations in plasmas, since the multi-fringe phase changes produced by a reflectometer are easily masked by those due to density fluctuations. Several methods have been proposed to avoid this problem such as amplitude-modulation (AM) reflectometry [1] or dual-frequency differential reflectometry [2] and pulsed-radar reflectometry using moderate short pulse [3] or ultrashort pulse [4] as well as

*Corresponding author's e-mail: mase@prc.tsukuba.ac.jp
※Present Address: National Institute for Fusion Science, Toki 509-5292, Japan
†この論文は第14回年会にて招待講演として発表されたものを論文化したものです.

advanced data processing techniques based on sliding Fast Fourier Transform (FFT) algorithms [5] and on maximum entropy method (MEM) [6].

We report here on two types of reflectometers, a broadband FM reflectometer and an ultrashort-pulse reflectometer. The source of the FM reflectometer for density profile measurement can be swept faster than the characteristic time scale of density fluctuations. The high-frequency fringes due to the change of frequency and the cutoff layer are distinguished from those due to the density fluctuations, since the fluctuation level with frequency larger than a few MHz is usually much smaller than the average density. Several different data processing techniques have been applied in order to reconstruct density profiles from the fringe data, that is, zero-cross counting method, digital complex demodulation (CDM) analysis [7], and spectral analysis using MEM [8] and wavelet transform [9]. Recently, an ultrashort-pulse reflectometer using an impulse oscillator (8 V amplitude and 65 ps pulse width) as a source has been applied to the central-cell plasma [10]. The Fourier component of the oscillator lies in the similar frequency range as the FM reflectometer.

The reflectometry has the distinct advantage of providing a local, nonperturbing measure of density fluctuations from edge to core regions of plasmas, which enables to monitor magnetohydrodynamic (MHD) behaviors, low-frequency instabilities, and ion cyclotron range of frequency (ICRF) waves [11-14]. In this paper, a broadband reflectometer with FM and fixed frequency operations is used to monitor the low-frequency instabilities and ICRF waves. The reflectometer is also utilized as a cross-polarization scattering (CPS) system for the measurement of magnetic fluctuations. The CPS is related to the mode conversion effect consisting of a polarization difference of a scattered wave from an incident wave by magnetic-field fluctuations [15,16]. It has been mentioned recently that magnetic fluctuations as well as density and potential fluctuations are of importance for plasma transport. The direct measurement of internal magnetic fluctuations becomes a major issue in plasma diagnostics. We have applied the CPS measurement to electromagnetic ICRF waves [17] and low-frequency waves [18].

2. Principles of Reflectometry

2.1 Density profile measurements

A reflectometer consists of a probing beam propagating through a plasma and a reference beam. The microwave beam in the plasma undergoes a phase shift with respect to the reference beam. This phase difference as a function of the probing frequency is given by

$$\phi(\omega) = 2k\int_{a}^{r_c(\omega)} \mu(r,\omega)\,\mathrm{d}r - \frac{\pi}{2} \tag{1}$$

within the WKB approximation, where k and ω are the wavenumber and frequency of the probing beam, μ is the plasma refractive index, and a and $r_c(\omega)$ are the plasma and cutoff radii, respectively. The refractive indices of the O-mode and the X-mode propagations are given by

$$\mu_O = \frac{ck_O}{\omega_O} = \left(1 - \frac{\omega_{pe}^2}{\omega_O^2}\right)^{1/2}, \tag{2}$$

$$\mu_X = \frac{ck_X}{\omega_X} = \left(1 - \frac{\omega_{pe}^2}{\omega_X^2}\cdot\frac{\omega_X^2 - \omega_{pe}^2}{\omega_X^2 - \omega_{pe}^2 - \omega_{ce}^2}\right)^{1/2} \tag{3}$$

in the cold plasma approximation, where c is the speed of light, ω_{pe} and ω_{ce} are the electron plasma frequency and the electron cyclotron frequency, and subscript O and X correspond to the ordinary mode and the extraordinary mode incident waves, respectively. For the O-mode propagation, this integral can be analytically solved for the density profile using an Abel inversion. For the X-mode propagation, a numerical algorithm has been developed to invert the data [19].

In an ultrashort-pulse reflectometer, a very short pulse (1 − 100 ps) is used as a probe beam. The pulse has a frequency component governed by the shape and duration. Each Fourier component reflects from a different spatial location in the plasma. The time-of-flight for a wave with frequency ω from the vacuum window position r_w to the reflection point at r_p is given by

$$\tau(\omega) = \frac{2}{c}\int_{r_w}^{r_p} \mathrm{d}r\left(1 - \frac{\omega_{pe}^2}{\omega^2}\right)^{-1/2}. \tag{4}$$

In order to obtain the density profile from the time-of-flight data, the Eq. (4) can be Abel inverted to obtain the position of the cutoff layer,

$$r(\omega_{pe}) = \frac{c}{\pi}\int_{0}^{\omega_{pe}} \frac{\tau(\omega)}{\left(\omega_{pe}^2 - \omega^2\right)^{1/2}}\,\mathrm{d}\omega\,. \tag{5}$$

By separating different frequency components of the reflected wave and obtaining time-of-flight measurement for each component, the density profile can be determined. The movement of the plasma position due to the fluctuations can be neglected during the reflection of ultrashort pulse (ps).

2.2 Fluctuation measurements

Reflectometry has also been used in order to study plasma fluctuations. The instataneous phase shift ϕ between the local beam and the reflected beam is expressed as $\phi = \phi_0 + \delta\phi$, where ϕ_0 and $\delta\phi$ are the phase shift depending on the cutoff layer due to density and density fluctuations of the plasma profile. In a simple homodyne reflectometer, the mixer output is given by

$$\begin{aligned} V &= E_l E_r \cos(\phi_0 + \delta\phi) \\ &= E_l E_r (\cos\phi_0 \cos\delta\phi - \sin\phi_0 \sin\delta\phi) \\ &\cong E_l E_r (\cos\phi_0 - \delta\phi \sin\phi_0) \end{aligned} \tag{6}$$

assuming $\delta\phi \ll 1$, where E_l and E_r are the electric field amplitude of the local beam and the reflected beam, respectively. The time varying component of the mixer output depends on both amplitude and phase modulations, since E_r can be time dependent due to changes in the cutoff layer. In general, the radial fluctuations of the cutoff layer produce the phase modulations and the poloidal (azimuthal) fluctuations cause amplitude modulations. Therefore it is important to identify both phase and amplitude fluctuations using, such as, heterodyne detection or quadrature type mixer [20].

In a simple one-dimensional model, the phase changes in the O-mode and the X-mode propagations due to the small perturbations of the density and the magnetic field, $\tilde{n}_e$ and $\tilde{B}$ at the critical density layer are given by [21]

$$\delta\phi_O \approx 2k_O L_n (\tilde{n}_e / n_e) \tag{7}$$

and

$$\delta\phi_X \approx \frac{2k_X \left[\, \tilde{n}_e/n_e + (\omega_{ce}\omega_X/\omega_{pe}^2)\tilde{B}/B \,\right]}{1/L_n + (\omega_{ce}\omega_X/\omega_{pe}^2)/L_B} \tag{8}$$

When the wavelength of the fluctuation is much longer than the spot size of the incident wave, there is no attenuation or modulation of the reflected wave. The depth of the phase modulation approaches the 1D geometric optics limit [22].

3. Description of Experimental Arrangements

3.1 GAMMA 10 tandem mirror

The present experiment is performed in the hot-ion mode of GAMMA 10 [23]. The ICRF power with frequencies of 9.9 MHz and 10.3 MHz (RF1) and 6.36 − 8.93 MHz (RF2) is employed to buildup a plasma and heat ions following gun-produced plasma injection. The frequency of 6.36 − 8.93 MHz corresponds to the ion cyclotron frequency near the midplane of the central cell, and 9.9 MHz and 10.3 MHz correspond to that of the anchor cells. Two separate 28 GHz gyrotrons are used in the plug/barrier cells in order to create the confining potentials. Fundamental electron cyclotron resonance heating (ECRH) occurs in the plug regions (ECRH-P) and second-harmonic ECRH occurs in the barrier regions (ECRH-B). Figure 1 shows an example of the hot-ion mode with the time sequence of the heating systems. In this case the ECRH power using a 28 GHz gyrotron is applied to the central-cell plasma (ECRH-C). The central-cell plasma parameters are as follows: the line density $n_c l_c = 4 - 5 \times 10^{13}$ cm^{-2} with an effective diameter of $l_c = 22 - 24$ cm, the electron temperature $T_e = 60 - 120$ eV, and the averaged ion temperature $T_i = 5 - 7$ keV. The magnetic field strength at the midplane of the central cell is $B_c = 0.40 - 0.57$ T, and the mirror ratio is 4.9.

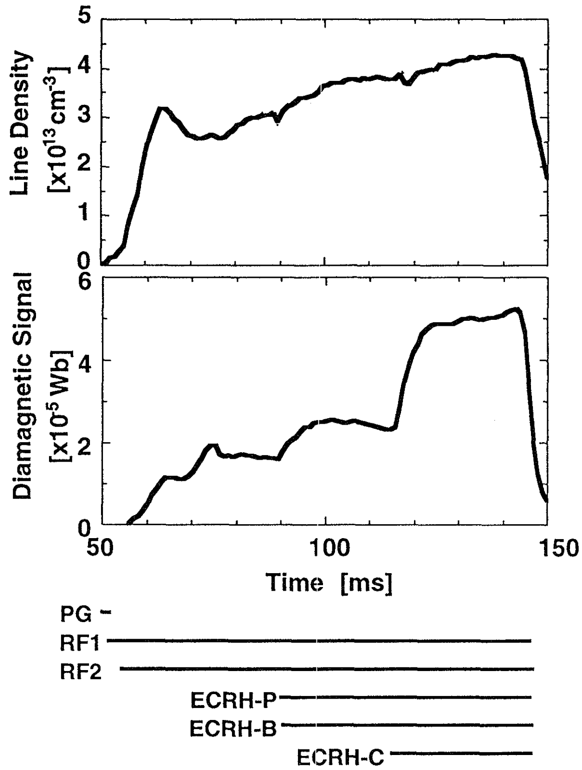

Fig. 1. Time evolution of the central-cell line density and diamagnetic-loop signal together with time sequence of the heating systems.

3.2 FM and ultrashort-pulse reflectometers for density profile measurement

The schematic of the FM reflectometer for diagnosing density profiles is shown in Fig. 2. It is installed in the central-cell midplane ($z = 0$ m). A hyperabrupt varactor-tuned oscillator (HTO) with 11.5 − 18 GHz and 40 mW output is used as a source. The separate transmitter and receiver horns are used to avoid the mixture of the spurious reflecting components in the waveguides and vacuum window. A focusing hog-horn antenna is used as a transmitter. The reflected wave picked up by a standard gain horn is mixed with the reference wave in a mixer through an 18 GHz low-pass filter. The homodyne-detected beat signals are then digitized at a sampling rate of 100 MHz with 128 kB memory using LeCroy 6841 digitizer or at a sampling rate of 50 MHz with 4 MB memory using Thamway AD-8H50II digitizer. In the present experiment the X mode propagation is adopted, since it covers a large portion of the density profile for the appropriate frequency range, 11.5 − 18 GHz.

We have applied and compared several reconstruction methods in order to obtain the density profiles, zero-cross counting of the fringes, digital phase

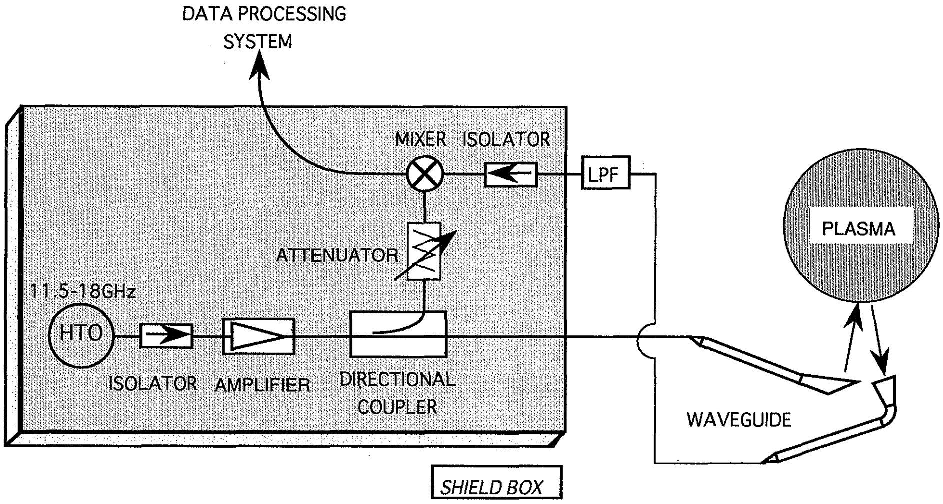

Fig. 2. Schematic diagram of the fast-sweep FM reflectometer.

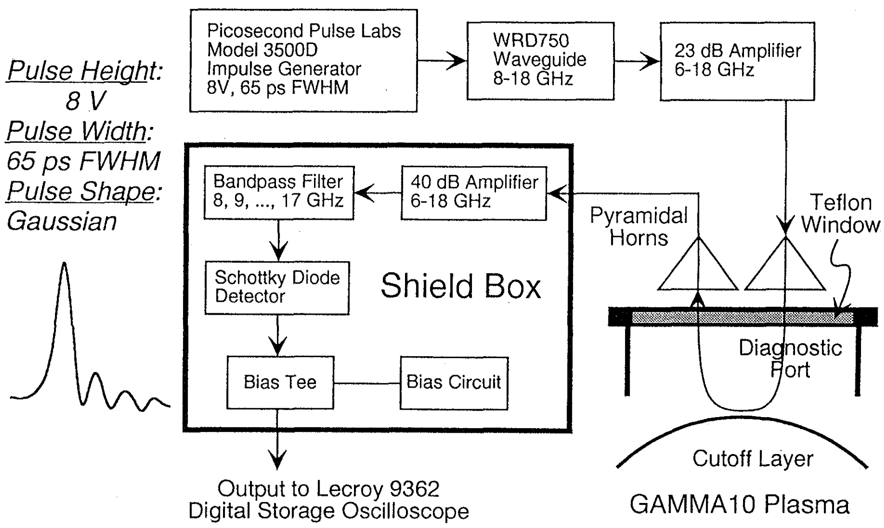

Fig. 3. Schematic diagram of the ultrashort-pulse reflectometer.

counting using complex demodulation technique (CDM), and frequency analysis by means of the MEM and wavelet.

A schematic of an ultrashort-pulse reflectometer (USPR) is shown in Fig. 3 [10]. The input source is an 8 V, 65 ps full-width half-maximum (FWHM) pulse. The impulse is fed through a 30 cm length of WRD750 waveguide which attenuates the low frequency part of the Fourier component, and streches into a chirped pulse. The resultant waveform is then amplified (6 − 18 GHz, 23 dB gain) before propagation via a pyramidal transmitter horn into a plasma with O-mode propagation. The received waveform picked up by an identical horn is amplified (6 − 18 GHz, 40 dB gain), and filtered. The filters have the center frequency 8 − 17 GHz with 1 GHz interval and 3% bandwidth of the center frequency. The output of each filter is rectified by a Schottky barrier diode detector, and fed to a LeCroy 9362 digital storage scope (sampling time 100 ps, bandwidth 750 MHz). Recently, constant fraction discriminators and time-to-amplitude converters (TACs) is also utilized. This system converts double-pass time delay data into analog voltages, and enables us to observe the time-of-flight of the pulse at 50 kHz − 1 MHz repetition rate with about 50 ps time resolution.

3.3 FM reflectometer and CPS diagnostic system for fluctuation measurements

The reflectometer and CPS diagnostic system for fluctuation measurements as shown in Fig. 4 are located at the midplane ($z = 0$ m) and at the west side ($z = 0.6$ and 1.8 m) of the central cell. At the central cell two pyramidal horns with O-mode and X-mode propagations are installed in the top and bottom diagnostic ports respectively, and used as a transmitter or a receiver for the reflectometer and the CPS measurement. The systems utilize an 8 − 18 GHz, 100 − 150 mW output of a yttrium-iron-garnet (YIG) sweep oscillator as a source. The YIG oscillator is operated in a fixed frequency mode during a plasma shot or a FM mode with 5 − 10 ms slow sweep rate. The reflected and/or scattered waves are mixed with the unperturbed local oscillator (LO) wave in a mixer. The intermediate frequency (IF) signal is amplified and separated into three ports by a power splitter. One of them is connected to a digitizer with 20 ns sampling time and 4 MB memory, while the others are fed to bandpass filters and rectified through detectors. The center frequencies of the bandpass filters are chosen to the frequencies of the RF2 and the self-excited instability identified as the Alfvén ion cyclotron (AIC) wave, respectively.

4. Experimental Results and Discussion

4.1 Density profiles

4.1.1 Reliability of density profile reconstruction in FM reflectometry

When the frequency of the incident wave is swept, multiradian phase change occurs due to the change of the cutoff layer and the path difference between the probe beam and the reference beam. The period of the fringes depends on the sweep speed of the source. Figure 5 shows a typical example of the density fluctuations obtained by a fixed-frequency reflectometer installed in the central cell. The low-frequency components with frequency less than 100 kHz are identified to

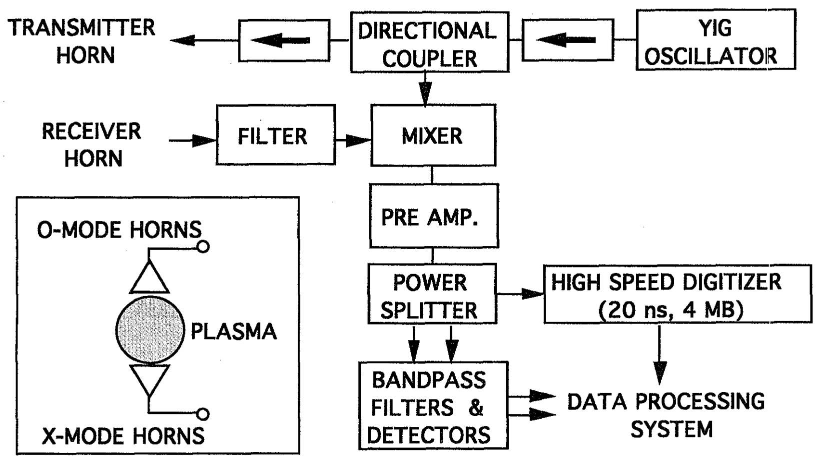

Fig. 4. Schematic diagram of the FM reflectometer and the CPS diagnostic system.

be flute-type and/or drift-wave modes by using a far-forward scattering system and probes. The high-frequency components with frequency 5 − 12 MHz are ICRF-driven waves such as the Alfvén ion cyclotron instability and the applied ICRF waves. The resultant intermediate frequency (IF) between the reflected and reference waves for each sweep time of the HTO is also shown in Fig. 5. When the HTO is swept in 5 ms, the frequency spectrum of the IF signal lies in the range of 1 − 100 kHz, which is almost the same as that of the strong low-frequency fluctuations excited in the central-cell plasma. Therefore, the fluctuations easily mask the information of the density profile.

The performance of the reflectometer system is investigated for various sweep times of the HTO. In Fig. 6, the density profile reconstructions are performed by using two phase extraction methods, zero-cross counting and digital phase counting using CDM. It is seen that the reconstructed density profiles seem to be improved when the sweep time is faster than 200 μs for the CDM, while the sweep time at least faster than 20 μs seems to be necessary for the zero-cross counting. The IF is in the range of > 0.8 MHz and > 8 MHz, respectively. Since the fluctuation level is much smaller than the average density ($\tilde{n}/n < 10^{-3}$) in this frequency range, it is easy to locate the fringes. In the previous paper, the zero-cross counting was compared to the MEM spectral analysis [24]. The results show that the improvement of data analysis is important for good profile reconstruction, however, it is also demonstrated that when the system performance is improved, such as fast sweeping, the demands on data analysis become lower.

Recently, the wavelet analysis is also introduced as an alternative to the MEM spectral analysis in order to obtain the good time-frequency resolution in signal processing. We have chosen the Gaussian wavelet as,

$$\psi_\omega(t) = \sqrt{\frac{\omega}{2\pi}}\exp(\mathrm{i}\omega t)\exp\left(-\frac{\omega^2 t^2}{8\pi^2}\right). \qquad (9)$$

Here, both the packet width and the wavelet frequency can be changed continuously by varying the value of ω. In order to determine the time-frequency dependence of the detected signal $s(t)$, we first normalize it in such a way that each data sequence of 100 points has a

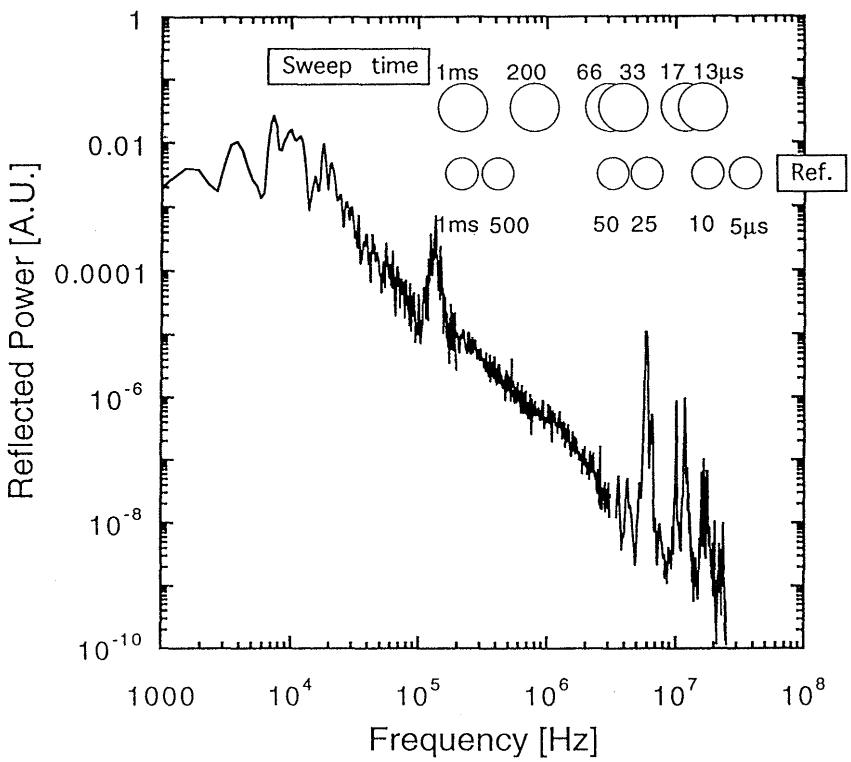

Fig. 5. Typical frequency spectrum of the density fluctuations at the central-cell plasma. The circles are resultant beat frequency between the reflected wave and the reference wave for each sweep time of the HTO.

zero-average value and a constant variance, and obtain a convolution with a wavelet function for different frequency

$$S(\omega,t)=\int s(\tau)\psi_{\omega}(t-\tau)\mathrm{d}\tau. \tag{10}$$

This gives the wavelet spectrum of the detected signal

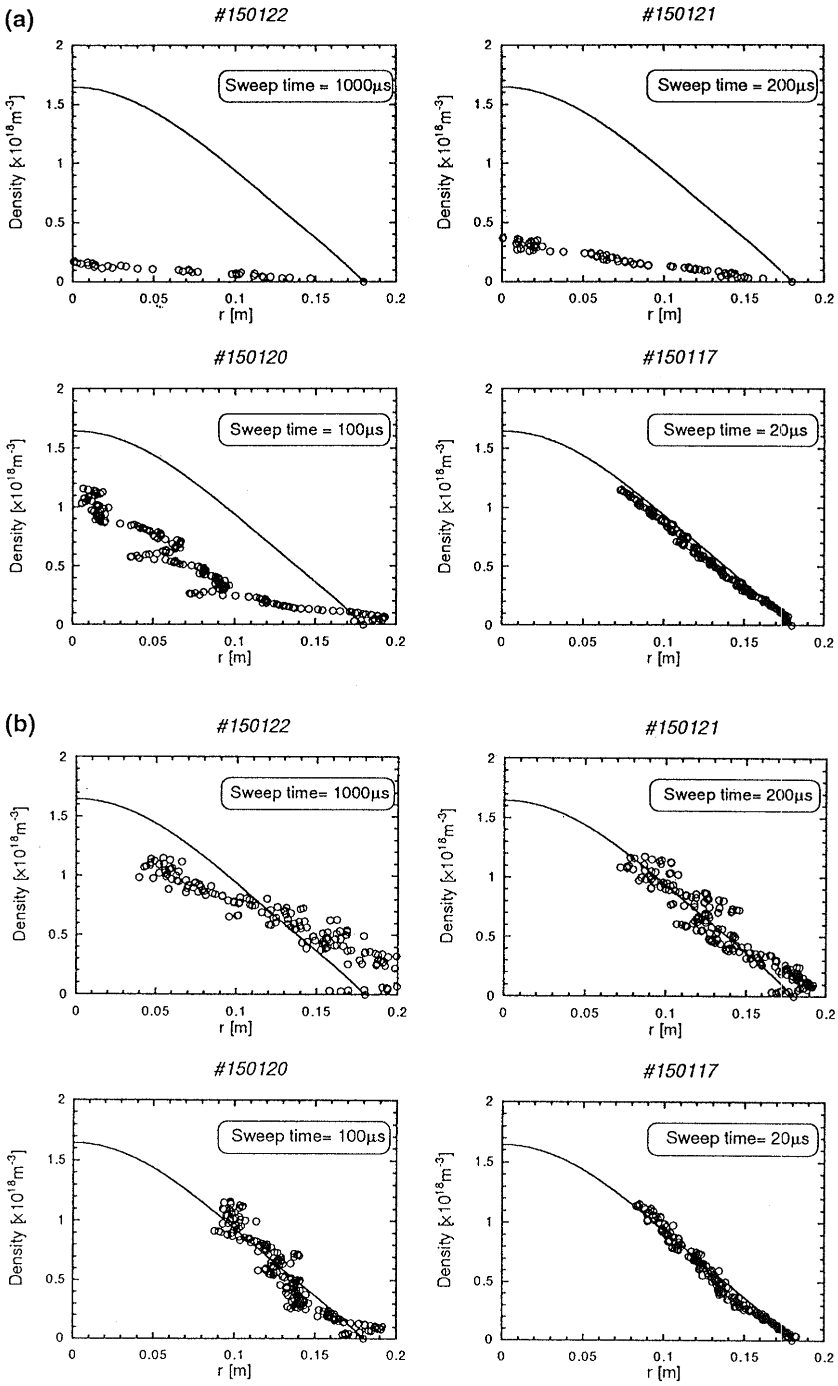

Fig. 6. Density profiles for various sweep times reconstructed by the zero-cross counting method (a) and the CDM method (b).

as shown in Fig. 7. It is possible to locate the maximum points and obtain the required time dependence of signal frequency. Typical density profiles obtained with present FM reflectometer are shown in Fig. 8. Here the sweep time of 20 μs is adopted. Note that we can obtain the density profiles for almost every sweep.

4.1.2 Time-of-flight measurement in ultrashort-pulse reflectometry

A proof-of-principle experiment of an ultrashort pulse reflectometry has been performed on GAMMA 10. Figure 9 shows a plot of the measured time-of-flight between the vacuum window and the cutoff layer of the plasma as a function of the Fourier component of the impulse. The fast-time digitizer with sampling time of 100 ps is used for this experiment. The calibration measurements are conducted with an aluminum plate placed on the surface of the vacuum window between plasma shot. Without the aluminum plate the reflection from the window surface is quite small, and does not interfere with the measurements of cutoff layer. The solid line is calculated from Eq. (4) using the Abel-inverted density profile from the scanning microwave interferometer. The observed time-of-flight is in good agreement to the interferometer data within the error bar. In the present system, the reflected signal for center frequency above 11 GHz is not clear, probably due to the small Fourier components in the 65 ps FWHM impulse, the long distance to the cutoff layer which causes divergence of the wave, and the shallow density gradient in the core plasma region which disperses the reflected wave.

4.2 Density and magnetic fluctuations

4.2.1 Measurement of ICRF-driven waves by FM reflectometry

The AC output of a homodyne reflectometer is proportional to phase fluctuations when the one-dimensional geometric optics model is assumed and the fluctuation level is much smaller than 1. In this experiment FM reflectometers have been applied to the measurements of ICRF-driven waves, since the ICRF waves have rather long wavelength (much longer than the incident wavelength), and are coherent. The fluctuation level is also much smaller than the low-frequency waves as shown in Fig. 5.

In the present experiment, the mixer output of the reflectometer is expressed by a combination of amplitude fluctuation $A(t)$, DC phase change by density profile ϕ_D, and phase fluctuations $\delta\phi_L$ and $\delta\phi_R$ due to the low-frequency and RF waves, respectively, as

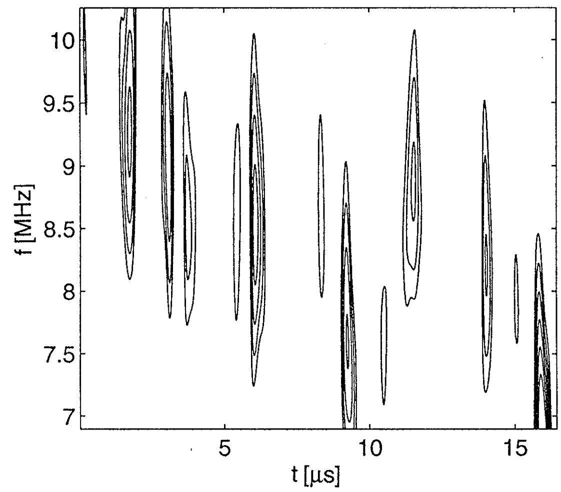

Fig. 7. Contour plot of the wavelet spectrum.

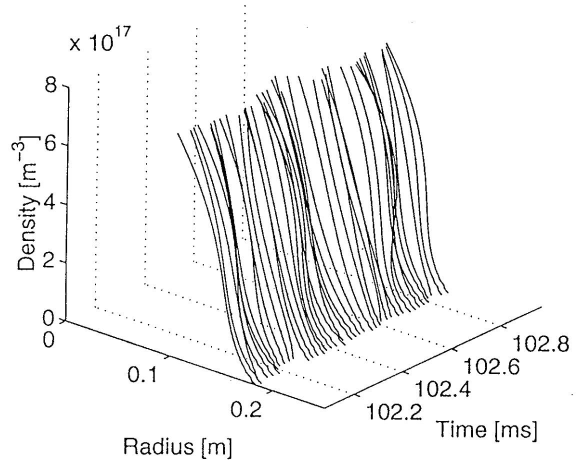

Fig. 8. Density profiles reconstructed by the wavelet analysis for many subsequent sweeps. The sweep time is 20 μs.

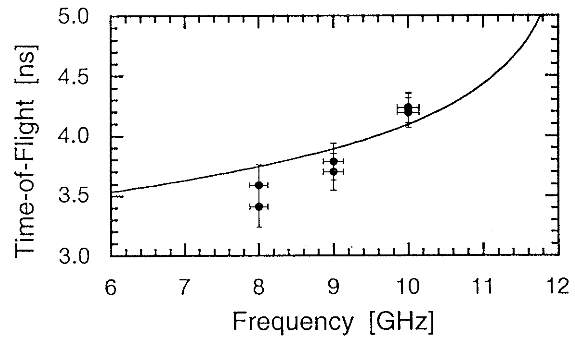

Fig. 9. Measured time-of-flight for various filters. The solid line represents the time-of-flight calculated from the Abel inversion of the interferometer data.

$$(1 + A(t))\sin(\phi_{\rm D} + \delta\phi_{\rm L} + \delta\phi_{\rm R})$$
$$= (1 + A(t))\,[\sin(\delta_{\rm D} + \delta\phi_{\rm L}) + \delta\phi_{\rm R}\cos(\phi_{\rm D} + \delta\phi_{\rm L})] \qquad (11)$$

assuming $\delta\phi_{\rm R} << 1$. Since the density fluctuation level due to the RF waves is estimated to be $\sim 10^{-4}$ and much smaller than that of the low-frequency waves, the contribution of the RF waves to $A(t)$ is negligible. The phase fluctuations are represented by

$$\delta\phi_{\rm L} = \sum_k A_k \sin \omega_k t,$$
$$\delta\phi_{\rm R} = A_{\rm RF} \cos \omega_{\rm RF} t + A_{\rm AIC} \cos \omega_{\rm AIC} t, \qquad (12)$$

where $\omega_{\rm RF}$ and $\omega_{\rm AIC}$ show the frequency of RF and AIC waves, respectively. The output after each band pass filter is expressed by the time-integration of square of $(1 + A(t))A_{\rm RF}\sin(\phi_{\rm D} + \delta\phi_{\rm L})$ or $(1 + A(t))A_{\rm AIC}\sin(\phi_{\rm D} + \delta\phi_{\rm L})$, and is proportional to $A_{\rm RF}^2/2$ and $A_{\rm AIC}^2/2$, respectively. Therefore, the reflectometer output is proportional to the density fluctuation of the RF waves $(\tilde{n}/n)^2$.

Figure 10 shows the radial profiles of the O-mode reflectometer output for various times. The density fluctuation level $(\tilde{n}/n)^2$ is linearly proportional to the RF power. It is noted that the RF2 is detected in the core plasma in the early stage of the discharge, however, it is detected more in the edge during the saturation of the diamagnetic pressure. On the other hand, the AIC mode localizes in the core plasma region due to the increase in the plasma β. This figure is obtained by scanning the YIG oscillator frequency in 10 − 20 ms.

4.2.2 Measurement of cross-polarization scattering

The CPS method has been applied to the measurements of low-frequency waves as well as the ICRF-driven waves. Two types of CPS can be observed by using horn antennas installed in the top and bottom ports, O- to X-mode (O → X) scattering and X- to O-mode (X → O) one. The time evolution of the frequency spectra is shown in Fig. 11. The frequency spectra of the CPS and the reflectometer signals show that the low-frequency waves less than 100 kHz is excited in a plasma. Figure 11 corresponds to the O → X mode CPS (incident frequency: 10.20 GHz) and the X-mode reflectometer (14.29 GHz) signals. The incident frequencies are chosen so that both systems observe the similar radial positions of the plasma at the same shot. It is seen that the intensity and spectra of the fluctuations are changed after the ECRH is applied, indicating

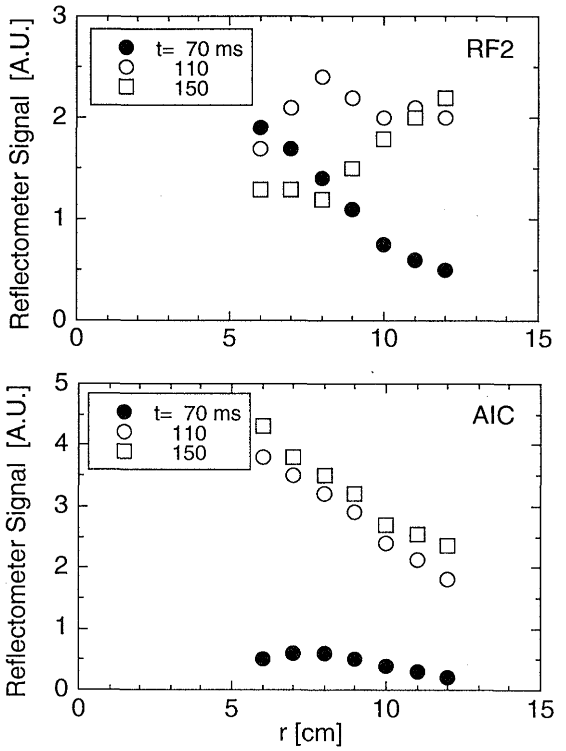

Fig. 10. Time evolution of the ICRF-wave distributions: ICRF heating wave (top), and AIC wave (bottom).

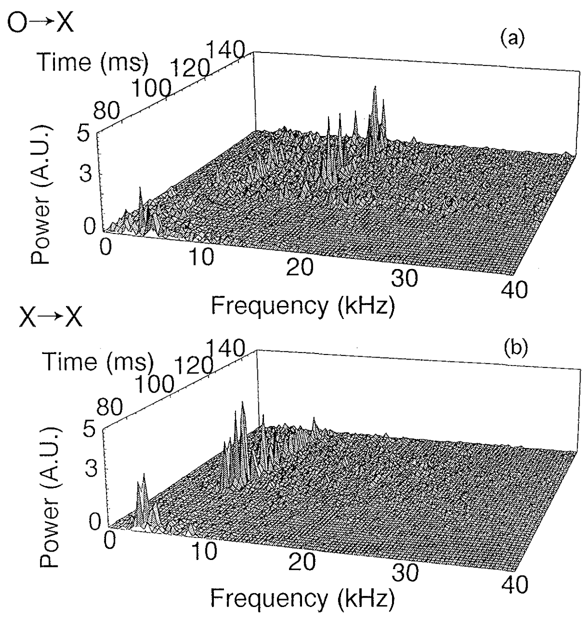

Fig. 11. Frequency spectrum of the CPS (O → X) signal (a) and the reflectometer (X → X) signal (b).

the modification of the radial electric field due to the potential formation. Note that the frequency spectrum of the CPS signal is broader than that of the reflectometer signal.

The discrepancy of the spectra between the CPS and the reflectometer signals can be explained as follows. The refractive indices of the O-mode and the X-mode propagations are given by Eqs. (2) and (3). In the CPS process, the incident O (X) wave is converted to the X (O) wave by the magnetic fluctuations until it reaches the cutoff layer of the plasma. The scattering process satisfies the wavenumber resonance condition (Bargg condition) $\boldsymbol{k} = \boldsymbol{k}_i - \boldsymbol{k}_s$, where $\boldsymbol{k}$, $\boldsymbol{k}_i$ and $\boldsymbol{k}_s$ are the wavenumber vectors of the fluctuation, the incident wave, and the scattered wave, respectively. Therefore, $k \cong 0$ in the transparent region of the plasma, since the scattering angle $\theta_s \cong 0$ for the present system and $k = 2k_i \sin(\theta_s/2)$, where $k_i \cong k_s$ is close to the wavenumber in the vacuum. At the cutoff region in the O → X process, the wavenumber of the incident wave, k_O becomes 0 from Eq. (2), however, that of the mode-converted X wave, k_X becomes ω_X/c from Eq. (3). In the X → O process, the wavenumber of the mode-converted O wave, k_O becomes $0.81\omega_O/c$ at the cutoff region in the same manner. As a result, k varies from 0 to k_i for the O → X process and from 0 to $0.81k_i$ for the X → O process. On the other hand, the reflectometer always gives $k \cong 0$, since the wavenumbers of the incident wave and the scattered wave equal to 0 at the cutoff layer. Since the frequency of the waves are usually given by the relation $\omega = kv_p$, where v_p is the phase velocity of the wave, we should observe the higher frequency in the CPS measurement. The phase velocity of the waves estimated from the observed spectra, $v_p \cong 5 - 10 \times 10^3$ m is in agreement with the drift velocity $v_d \cong T_e/eBL_n$ using the present experimental conditions, where e is the charge of an electron and L_n is the density scale length. The magnetic field fluctuations may have significant influence in the drift-wave mode due to the finite-β effect and the shearless magnetic filed of a tandem mirror, i.e. $(4\pi n_e T_e/B^2)(L_s^2/L_n^2) > 1$, where L_s is the shear length of the magnetic field [25].

4.2.3 Possibility of simultaneous measurement of density and density fluctuations using ultrashort-pulse reflectometry

The ultrashort-pulse reflectometer using constant fraction discriminators and time-to-amplitude converters (TACs) will be suited to follow changes in the electron density profile that result from induced perturbations. The system enables us to observe the time-of-flight of the pulse at the maximum repetition rate of 1 MHz with 30 psec time resolution. Figure 12 shows the time evolution of the flight time of the 10 GHz output at $t = 90$ ms together with the frequency spectra of the far-forward scattering signal. It is seen that the position of the critical density layer of the plasma ($r/a \cong 0.6$, where a is the plasma radius) is oscillating. The time resolution of the system is estimated to be about 50 ps from the deviation of the flight time when an aluminum plate is used as a reflector. The period of the oscillation agrees with the frequency peak of the scattered signal at 90 ms. The normalized density fluctuation is estimated to be 15 − 20% from the time-of-flight data.

5. Summary

In summary, an ultrafast-swept reflectometer has been applied to the central cell of the GAMMA 10 tandem mirror. The reliability of the density profile measurement is investigated for various sweep times of the source (HTO) from 10 μs to 1 ms. It is observed that the reconstructed density profile is highly improved when the sweep time is faster than 100 − 200 μs for the digital phase counting using the CDM method, while it has to be faster than 20 μs for the zero-cross counting method. Although the improvement of data analysis is important for the good profile reconstruction, it is also demonstrated that when the system performance is improved, such as fast sweeping, the demands on data analysis become lower. The wavelet transform provides very good time-frequency resolution as well as having a denoising capability, and is quite useful for the profile reconstruction method of reflectometry. It is possible to obtain the density profiles for almost every sweeps in 20 μs.

The FM reflectometry and the cross-polarization scattering diagnostic method with frequency of 7 − 18 GHz has also been applied to the central-cell plasma for measurement of density/magnetic fluctuations in the ICRF-driven and the low-frequency waves. The time evolution of RF-wave profiles are obtained in a single shot for the first time. The CPS signals (both O → X and X → O scattering) exhibit the broader frequency spectra than those of the reflectometer signals, which is considered to be the satisfaction of the Bragg resonance condition.

The proof-of-principle experiment of the ultrashort-pulse reflectometry using 65 ps and 8 V FWHM impulse has been carried out. The observed values of the time-of-flight are in agreement with those calculated using the Abel-inverted profile from the ineterferometry data. The possibility of simultaneous

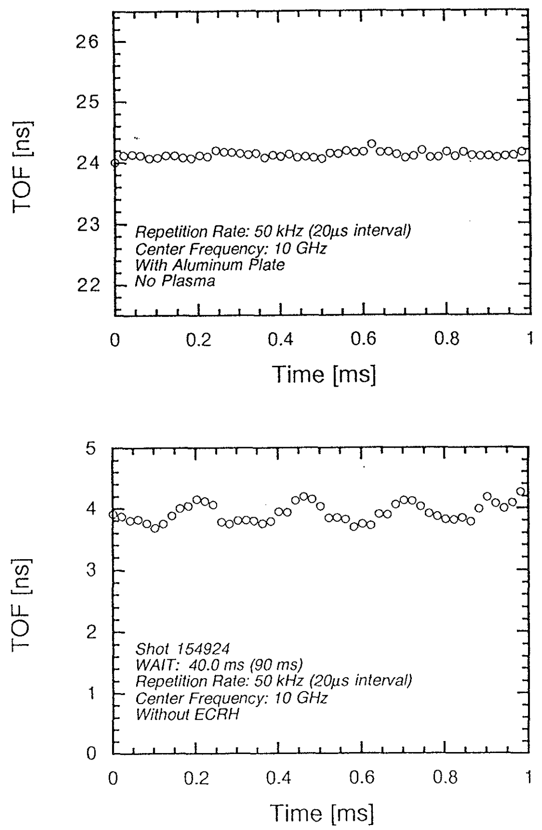

(a)

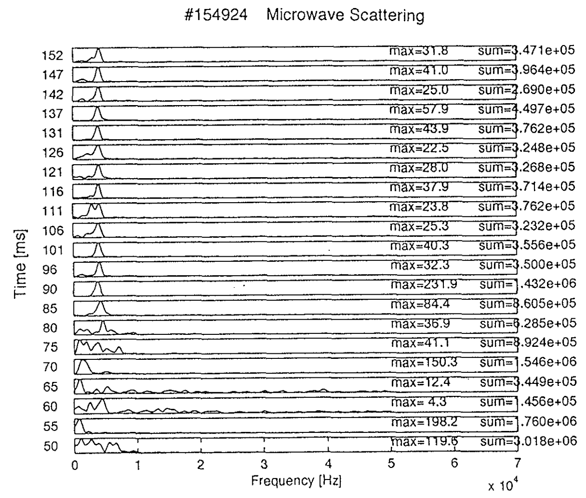

(b)

Fig. 12. (a) Time evolution of the flight time measured with the TAC system: reflection from the aluminum (top) and the plasma (bottom). The repetition rate of the impulse is 50 kHz. (b) Spectrum of the far-forward scattering signal.

measurements of density profile and density fluctuations is demonstrated.

Acknowledgments

The authors deeply acknowledge the members of GAMMA 10 group for their collaboration. This work was supported in part by a Grant-in-Aid for Scientific Research from the Japanese Ministry of Education, Science, Sports and Culture.

References

[1] J. Sánchez, B. Branas, T. Estrada, E. de la Luna and V. Zhuravlev, Rev. Sci. Instrum. **63**, 4654 (1992).

[2] G.R. Hanson, J.B. Wilgen, T.S. Bigelow, I. Collazo, A.C. England, M. Murakami, D.A. Ramussen and J.R. Wilson, Rev. Sci. Instrum. **66**, 863 (1995).

[3] A.J.H. Donné, S.H. Heijnen and C.A.J. Hugenholtz, Fusion Eng. Des. **34–35**, 73 (1997).

[4] C.W. Domier, N.C. Luhmann Jr., A. Chou, W-M. Zhang and A.J. Romanowsky, Rev. Sci. Instrum. **66**, 399 (1995).

[5] J. Santos, M. Manso, F. Nunes, I. Nunes, A. Silva and O. Varela, *Proc. 3rd Workshop on Microwave Reflectometry for Fusion Plasma Diagnostics*, Madrid (1997) p.55.

[6] M. Nagatsu, T. Hayashi, Y. Matsushita and T. Tsukishima, Jpn. J. Appl. Phys. **33**, L45 (1994).

[7] K.W. Kim, E.J. Doyle, W.A. Peebles, A. Ejiri, N.C. Luhmann Jr. and C.L. Rettig, Rev. Sci. Instrum. **66**, 1229 (1995).

[8] M. Nagatsu, A. Fuse and A. Mase, Plasma Phys. Control. Fusion **38**, 1033 (1996).

[9] L.G. Bruskin, A. Mase, T. Tokuzawa, N. Oyama, A. Itakura and T. Tamano, Jpn. J. Appl. Phys. **36**, L632 (1997).

[10] S. Kubota, T. Onuma, A. Mase, T. Tokuzawa, L.G. Bruskin, N. Oyama, A. Itakura, H. Hojo, T. Tamano, K. Yatsu, C.W. Domier and N.C. Luhmann Jr., Jpn. J. Appl. **37**, L300 (1997).

[11] E. Mazzucato and R. Nazikian, Phys. Rev. Lett. **71**, 1840 (1993).

[12] T.L. Rhodes, W.A. Peebles, E.J. Doyle, P. Pribyl, M. Gilmore, R.A. Moyer and R.D. Lehmer, Plasma Phys. Control. Fusion **40**, 493 (1998).

[13] A. Mase, M. Ichimura, H. Satake, R. Katsumata, T. Tokuzawa, Y. Ito, H. Hojo, E.J. Doyle, A. Itakura, M. Inutake and T. Tamano, Phys. Fluids B **5**, 1677 (1993).

[14] J.H. Lee, W.A. Peebles, E.F. Jaeger, E.J. Doyle, N.C. Luhmann Jr., C.C. Petty, R.I. Pinsker, R. Prater and T.L. Rhodes, Phys. Rev. Lett. **80**, 2330 (1998).
[15] X.L. Zou, L. Colas, M. Paume, J.M. Chareau, L. Laurent, P. Devynck and D. Gresillon, Phys. Rev. Lett. **75**, 1090 (1995).
[16] L.G. Bruskin, A. Mase and T. Tamano, Plasma, Phys. Control. Fusion **37**, 255 (1995).
[17] A. Mase, L.G. Bruskin, N. Oyama, T. Tokuzawa, H. Inutake, A. Itakura, H. Hojo, M. Ichimura and T. Tamano, Rev. Sci. Instrum. **68**, 454 (1997).
[18] Y. Kogi, A. Mase, L.G. Bruskin, N. Oyama, T. Tokuzawa, A. Itakura, H. Hojo and T. Tamano, Jpn. J. Appl. Phys. **36**, L587 (1997).
[19] E.J. Doyle, T. Lehecka, N.C. Luhmann Jr., W.A. Peebles and the DIII-D Group, Rev. Sci. Instrum. **61**, 2896 (1990).
[20] K. Shinohara, S. Shiraiwa, K. Hoshino, Y. Miura, K. Hanada, H. Toyama and JFT-2M Group, Jpn. J. Appl. Phys. **36**, 7367 (1997).
[21] N. Bretz, Phys. Fluids B **4**, 2414 (1992).
[22] G.D. Conway, *Proc. 3rd Workshop on Microwave Reflectometry for Fusion Plasma Diagnostics*, Madrid (1997) p.39.
[23] T. Tamano, Phys. Plasmas **2**, 2321 (1995).
[24] T. Tokuzawa, A. Mase, N. Oyama, A. Itakura and T. Tamano, Rev. Sci. Instrum. **68**, 443 (1997).
[25] S.J. Camargo, B.D. Scott and D. Biskamp, Phys. Plasmas **3**, 3912 (1996).